Results in Physics 24 (2021) 104129

Contents lists available at ScienceDirect

Results in Physics

journal homepage: www.elsevier.com/locate/rinp

All-dielectric refractive index sensor based on Fano resonance with high sensitivity in the mid-infrared region

Yuhao Zhang [a,b], Zhongzhu Liang [a,b,c,*], Dejia Meng [a], Zheng Qin [a,b], Yandong Fan [a,b], Xiaoyan Shi [a,b], David R. Smith [d], Enzhu Hou [c]

[a] State Key Laboratory of Applied Optics, Changchun Institute of Optics, Fine Mechanics and Physics, Chinese Academy of Sciences, Changchun, Jilin 130033, China
[b] University of the Chinese Academy of Sciences, Beijing 100049, China
[c] Center for Advanced Optoelectronic Functional Materials Research and Key Laboratory of UV Light-Emitting Materials and Technology of Ministry of Education, College of Physics, Northeast Normal University, Changchun 130024, China
[d] Center for Metamaterials and Integrated Plasmonics, Duke University, Durham, NC 27708, USA

ARTICLE INFO

Keywords:
Refractive index sensor
All-dielectric
Fano resonance
Mid-infrared region

ABSTRACT

We design and numerically analyze a Fano resonance device based on periodical all-dielectric "lucky knot" shaped nanostructure in the mid-infrared region with high sensitivity, which is insensitive to polarization and incident angle. The proposed nanostructure is sensitive to the change of the refractive index of the substance to be tested. We established the correspondence between the change of the refractive index and the peak position of the reflection spectrum. And then we propose an optical refractive index sensor with a sensitivity of 986 nm/RIU, and a maximum figure of merit of 32.7, which is much higher compared to the sensor based on metallic materials. The maximum Q-factor can reach 520. This study may provide a further step in optical sensing, biosensing and environmental monitoring.

Introduction

Mid-infrared spectroscopy is capable of detecting and identifying many kinds of molecules, such as DNA, protein and lipid, which are induced by various vibrational modes of material microstructures [1–2]. Due to the detecting label-free features, sensors based on metamaterials working in the mid-infrared region have been proposed in many fields of molecular vibrational modes sensing, bio-chemical sensing, RI index sensing and temperature sensing [3–7]. For example, a plasmonic metal–insulator-metal waveguide mid-infrared sensor was proposed with a sensitivity (S) of 5140 nm/RIU in 2019 [6]. The sensitivity of it may higher than most of plasmonic sensors, but the oscillation of free electrons in metallic materials such as gold and silver will cause strong radiation loss and local heating [8–9], which will broaden the resonance linewidth [10–11] leading to extremely low figure of merit (FoM) and quality (Q) factor, and may also alter the composition of the substance to be tested [12]. Moreover, metals are prone to oxidation and corrosion under high temperatures which limit their applications in harsh environments [13]. Due to the dielectric materials can avoid ohmic loss, all-dielectric nanostructures with much narrower linewidth stand out as strong candidate for sensing as a consequence. For instance, an asymmetric silicon nano-bar pairs based on Si are proposed in 2013, which exhibits a sharp resonance in the near-IR wavelength range [14]. Then in 2014, the author proposed split bar resonators based on Si with a potential sensitivity of 525 nm/RIU as an optical refractive index sensor [15]. In 2019, a nanocavity-based elliptical-hole photonic crystal composed of silicon for mid-infrared liquid sensing was suggested [7]. The Q factor of 10^4 can be achieved however the sensitivity is only 285 nm/RIU simultaneously. Recently, mid-infrared sensors with angle modulation based on graphene layers seem to be the best choice which leads to better sensitivity and spectral resolution with reduced absorption loss [3,16]. However, the production of graphene is immature and the cost is high, which seriously restricts their practical application [13,17,18]. Not only that, most of the sensors are sensitive to the polarization directions and incident angle of the light. Improving these two characteristics will be more conducive to the realization of portable fast sensing. Therefore, the focus of current research is designing a mid-infrared sensor with improving S and FoM, which is insensitive to polarization and incident angle simultaneously.

The Fano resonance-based metamaterials, due to their excellent

* Corresponding author at: State Key Laboratory of Applied Optics, Changchun Institute of Optics, Fine Mechanics and Physics, Chinese Academy of Sciences, Changchun, Jilin 130033, China.
E-mail address: liangzz@ciomp.ac.cn (Z. Liang).

https://doi.org/10.1016/j.rinp.2021.104129
Received 17 February 2021; Received in revised form 19 March 2021; Accepted 24 March 2021
Available online 31 March 2021

optical properties such as narrow linewidth and large local field enhancement, which can greatly improve the performance of the devices, have gradually become a development trend in the field light regulation [19–23]. Most Fano resonance are realized in the nanostructure of metal materials, and their spectral response is in the visible and near-infrared bands instead of mid-infrared region [24–26]. Recently, Fano resonance based on all-dielectric nanostructure has also attracted great attention [27]. These nanostructures not only have lower losses but also can excite the strong magnetic dipoles besides the electric dipoles. The optical field is mainly bound inside the device, which is beneficial to enhance the interaction between the optical field and the dielectric material achieving higher field enhancement [28]. In addition, the fabrication process of all-dielectric nanostructures can be simpler, which makes it possible to provide a new way for the realization of high-performance, miniaturization and high-integration photonic devices [29].

Based on the above situation, we designed a “lucky knot” shaped nanostructure based on all-dielectric materials, and analyzed resonance characteristics through FDTD method. Combining the narrow resonance line-widths, we proposed an optical refractive index (RI) sensor which can maintain a sensitivity (S) of 986 nm/RIU and a maximum FoM of 32.7 in the mid-infrared region. It shows additional advantages of being insensitive and independent to the polarization and the angle of the incident light. This study may provide a further step in the development of optical sensing, biosensing, safety inspection, environmental monitoring and other fields.

Design & theoretical analysis

The schematic of the designed “lucky knot” shaped nanostructure is shown in Fig. 1. The nanostructure is formed from a periodic unit cell made of crossed rods resonator and four ring resonators, both formed from Si. As shown in Fig. 1(b), P is the length parameter of the periodic “lucky knot”, where $P = 6\mu m$. L_1 and L_2 are the length and width parameters of the crossed rods respectively, where $L_1 = 0.6\mu m$, $L_2 = 5.6\mu m$. R and r are the outer and inner radius of the rings structure respectively, where $R = 1\mu m$, $r = 0.5\mu m$. The heights of the rods and rings are equal, which expressed as $t = 1\mu m$. The designed “lucky knot” nanostructure is fabricated on a BaF_2 substrate (due to the transmittance of BaF_2 is 90% in the mid-infrared region and its loss is small), and the RI of BaF_2 is 1.43. In order to evaluate the performance of the designed “lucky knot” structure, we adopt a finite-difference time-domain (FDTD) method to simulate the reflection spectrum. The dielectric function of simulated Si is taken from the empirically defined values by Palik [30]. The reflection performance is evaluated from a plane wave, which is incident on the surface of the “lucky knot” with the electric field polarized along x-axis as shown in Fig. 1(a). Perfectly matched layer (PML) boundaries are employed along z-axis and periodic boundaries are employed for the × and y axes. The unit cell geometry is approximated using a tetrahedral mesh. The simulated reflection spectrum is shown in Fig. 1 (c), where the inset is zoomed in at the narrow reflection band. It shows clearly that the proposed nanostructure can achieve perfect reflection at the wavelength of 7.3 μm with a bandwidth of 14 nm resulting in a Q factor as high as 520.

The High-Q resonance is realized by employing Fano resonance, which is relied on a “bright” mode resonator and a “dark” mode resonator [28]. The simulated near-field distribution at the resonance wavelength (7.3 μm) using FDTD method is plotted in Fig. 2. The crossed rods resonator couples strongly to free-space excitation with the incident E-field. The collective oscillations of the crossed rods resonators form the “bright” mode resonance. The rings are less-accessible from free

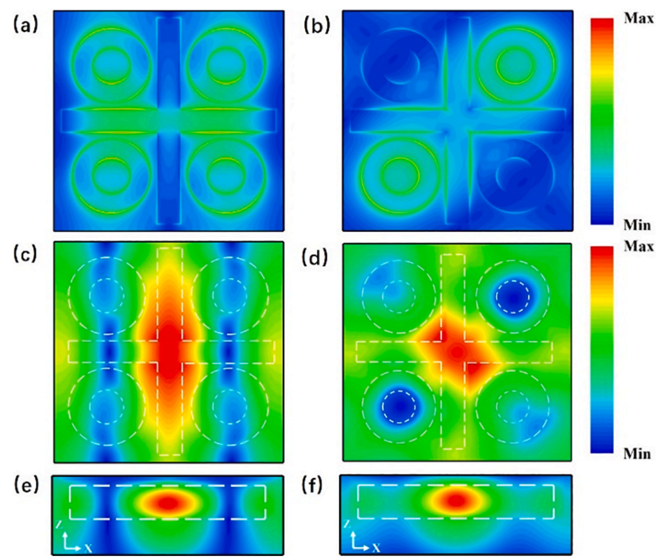

Fig. 2. Schematic diagram of near-field distribution at the resonance wavelength. Electric-field distribution in the x-y plane (a) when the electric field of incidence oriented along x-axis and (b) when the incident angle is 45 degrees. Magnetic-field distribution in the x-y plane (c) when the electric field of incident light oriented along x-axis and (d) when the incident angle is 45 degrees. Magnetic-field distribution in the x-z plane (e) when the electric field of incident light oriented along x-axis and (f) when the incident angle is 45 degrees.

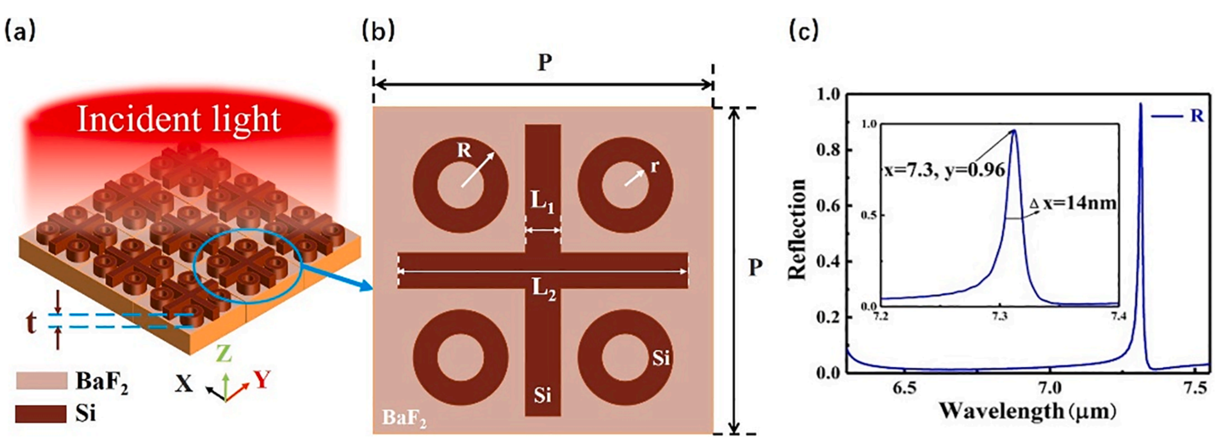

Fig. 1. (a) Schematic diagram of the proposed “lucky knot” shaped nanostructure and the incident light polarization configuration. (b) Top view of the “lucky knot” structure. The structure consists of a periodic array of dielectric substrates made of BaF_2 and the “lucky knot” shaped structure made of Si. The geometrical parameters are $P = 6$ μm, $L_1 = 0.6$ μm, $L_2 = 5.6$ μm, $R = 1$ μm, $r = 0.5$ μm, and $t = 1$ μm. (c) The reflection spectrum of the “lucky knot” at incidence of a plane wave with the electric field oriented along x-axis (when the incident angle is 0 degree). Insert shows an enlarged view of the resonance.

space but they can couple to the bright-mode crossed rods resonators. They can support a magnetic dipole mode and interact through near-field coupling, resulting in collective oscillation of the resonators, forming the "dark" mode of the system [31]. These two resonances are brought in close proximity in both spatial and frequency domains resulting in an extremely narrow reflection window as shown in Fig. 1 (b).

Fig. 2 (a), (c) are the electric-field and the magnetic-field distribution at 7.3 μm on the x-y plane respectively when the electric-field of the incident light polarized along the x-axis. And Fig. 2 (e) shows the magnetic-field distribution on the x-z plane. Unlike the localized surface plasmon using metallic, there is only electrical resonance and the field enhancement is mainly concentrated on the surface of the structure. High-RI dielectric particles exhibit magnetic and electric dipole and higher order Mie resonance when the incident electromagnetic wave irradiate. And due to the array effect of the period array structure, the far-field radiation of electromagnetic wave is hindered, so that the energy can be tightly bound inside the nanostructure. Fig. 2 (b) (d) (f) shows the electric-field and magnetic-field distribution at 7.3 μm when the polarization angle of the incident light is 45 degrees. Due to the rotational symmetry of the "lucky knot" structure, the resonance of the designed all-dielectric nanostructure is insensitive to the polarization direction of the incident light. In addition, it is independent to the incident angle of the light too. We define the incident angle is zero as the light shown in Fig. 1 (a) and it's for TM wave at oblique incidence. We simulate the incident angle changes from 0 to 45 degrees with a step of 5. It can be seen from the Fig. 3 that the peak position of the reflection spectra hardly changes when the incident angle changes. The full width at half-maximum (FWHM) of the reflection spectra is shown in table. 1. As the incident angle increases, the FWHM does not change significantly. And at the same time, the reflectance is maintained at approximately 95%.

At the same time, the proposed all-dielectric nanostructure is sensitive to changes in the RI of the surrounding environment. In the next part of this paper, we discuss the potential application of the proposed nanostructure for optical RI sensors.

Results and discussion

Due to the extremely narrow line width, one of the applications of this nanostructure design is optical RI sensor. The all-dielectric "lucky knot" shaped nanostructure proposed in this paper is sensitive to the changes in the RI. Fig. 4 shows a schematic diagram of the substance to be tested. By using FDTD method, we characterize the performance of the proposed RI sensor utilizing parameters including RI range and sensing resolution, sensitivity (denoted by symbol S), figure of merit (FoM), quality factor (Q) and dephasing time. Then we listed the performance between the RI sensor proposed in this work and sensors based on Fano resonance in the last five years.

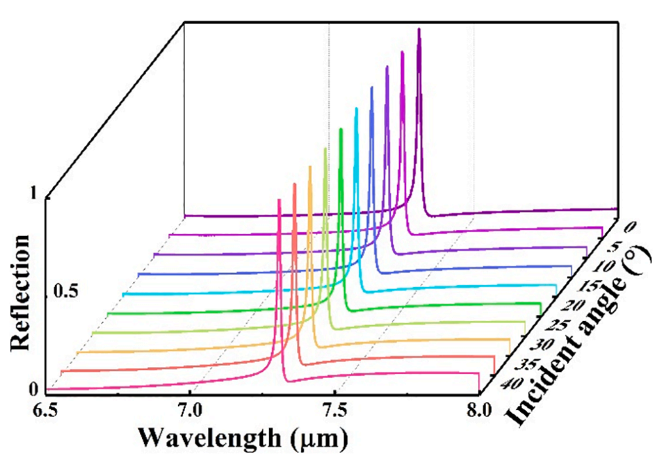

Fig. 3. The reflection spectra when the incident angle changes from 0 to 45 degrees with a step of 5.

Table 1
The full width at half-maximum (FWHM) of the reflection spectra at different incident angle.

Incident Angle (°)	0	5	10	15	20	25	30	35	40	45
FWHM (nm)	14	14	14	14	14	14	14	14	14	15

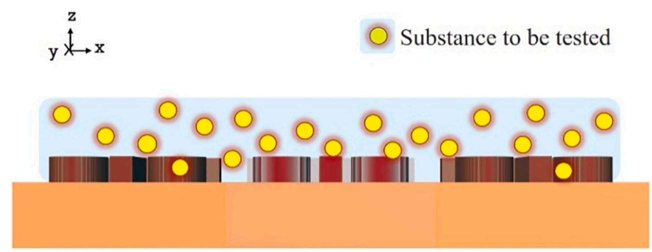

Fig. 4. Schematic diagram of the substance to be tested.

RI range and sensing resolution

Firstly, we investigate the RI range and sensing resolution of the proposed sensor. Fig. 5 (a) shows the reflection map as a function of the resonance wavelength and RI of the substance shown in Fig. 4 changes from 1.33 to 2.0 and an enlarged view from 1.33 to 1.40 in Fig. 5 (b). As observed from reflection maps, the wavelength of maximum reflectance has a significant increase as RI of the substance enlarges from 1.33 to 2.0. The higher the RI, the more obvious the movement of the wavelength. This feature can be observed more explicitly by the map shown in Fig. 5 (b) that is the RI of the substance has a liner relationship with the wavelength of the resonance. Compared with other RI sensors, our proposed sensor has a larger RI range, and it is worth noting that the RI range is not limited to the above. In addition, the sensing resolution of the proposed RI sensor can be lower than 0.001. As shown in Fig. 5 (c), a slight change in the RI can also cause a clearly shift in the resonant peak position.

Sensitivity

Generally, an important parameter to describe and compare the performance of optical RI sensors is sensitivity (S), which represents the shift of the resonance peak position per unit RI change, which is usually defined by the following formula [30]:

$$S = \frac{\Delta\lambda}{\Delta n} \tag{1}$$

where Δn represents the change in RI, and $\Delta\lambda$ represents the shift of the peak position of the resonance. By using FDTD method, we simulated the reflection spectra of the RI of the substance to be tested from 1.33 to 1.40 with a change step of 0.005. The result is shown in Fig. 6 (a). As RI of the substance to be tested increases, the position of the resonance peak shows a significant red shift phenomenon and the reflectance maintains above 98% at the same time. According to the results obtained in Fig. 6 (a), the movement of the peak position with the change in RI is shown in Fig. 6 (b).

The blue dotted line in Fig. 6 (b) is the relationship between RI and the peak position of resonance obtained by simulation, and the red dashed line is the fitted curve. It can be known that the RI has a linear relationship with the peak position of the resonance. According to the equation (1), the slope of the fitted curve is the sensitivity of the designed RI sensor. And the sensitivity is 981 nm/RIU which is much higher than the nanostructure based on metal materials. In addition,

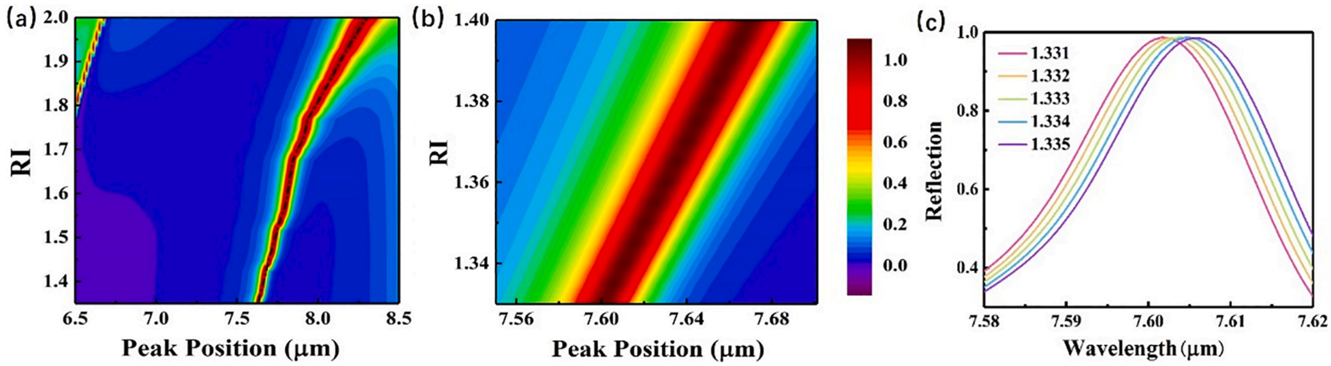

Fig. 5. Reflection map of the proposed sensor for the RI of substance changes from (a) 1.33 to 2.0 and (b) 1.33 to1.40 respectively. (c) The reflection spectra when the RI changing step is 0.001.

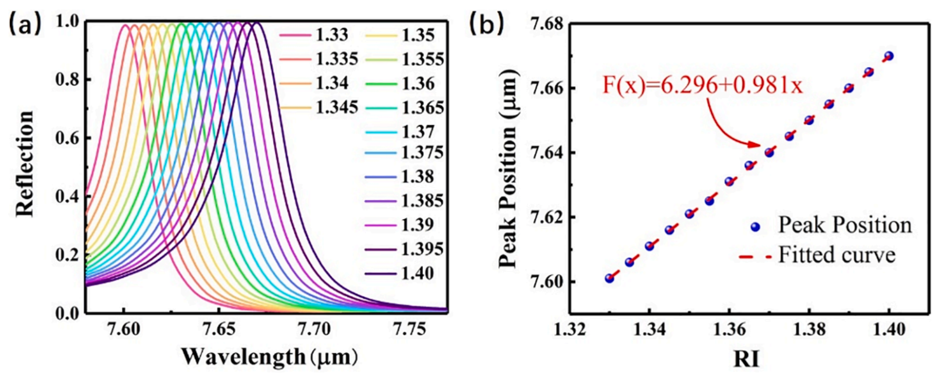

Fig. 6. (a) The reflection spectra when the RI changes from 1.33 to 1.40. (b) The curve of peak position with RI changes (blue dotted line) and fitted curve (red dashed line). (For interpretation of the references to colour in this figure legend, the reader is referred to the web version of this article.)

according to Fig. 5 (a), the sensitivity can increase when RI of the substance getting larger.

Figure of merit and Q factor

Aside from sensitivity, other important parameters to evaluate the performance of a RI sensor is the figure of merit (FoM) and Q factor, which are determined by the full width at half-maximum (FWHM), the sensitivity (S) and the wavelength of the resonance (λ) [32]: $\mathrm{FoM} = \frac{S}{FWHM}$ and $Q = \frac{\lambda}{FWHM}$. Generally larger FoM and Q factor is desired. Fig. 7 shows the FoM and Q factors of the RI sensor proposed in this paper.

It can be seen from Fig. 5 that the FoM of the designed RI sensor can reach up to 32.7 RIU^{-1}. As the RI increases, the FoM decreases, but the average value remains stable at 29 RIU^{-1}. The FoM of the RI sensor based on the local surface plasmon resonance of metallic nanoparticles

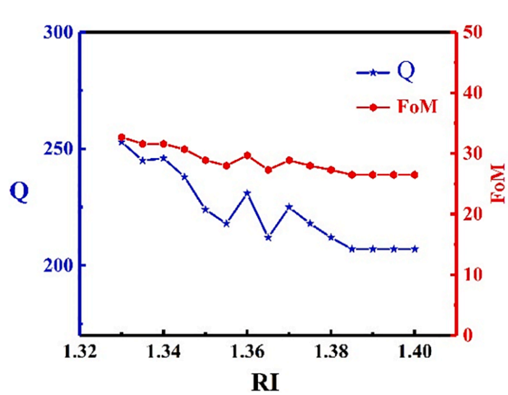

Fig. 7. The FoM and Q factor of the RI sensor as a function of RI.

is generally very low, mostly less than 5 RIU^{-1} due to the inherent loss of the metallic material. Dielectric materials instead of metal materials in our design can effectively improve the FoM value. An average Q remains 220 as the RI of the substance increases. The decrease of Q is due to the slightly increase of the FWHM caused by substance.

Dephasing time

In addition to the parameters mentioned in the section 3.1–3.3, we also calculated the dephasing time of the proposed dielectric nanostructure. Microscopically, the dephasing time is controlled by coupling of the resonance to the electron-hole pair continuum, and by radiation damping, which is important in large particles above a radius of ca. 10 nm [33]. It is a critical parameter that can be defined by taking to account of the resonance narrowness as following [33]: $T = 2\hbar/\delta$. Here, $\hbar$ is the reduced Planck's constant and δ is the homogeneous linewidth of the resonance. For the resonance at 7.3 μm (41.1 THz), the dephasing time is estimated as 1.8 ps.

In order to better analyze the performance of our proposed RI sensor, we list several RI sensors based on Fano resonance in the last five years, which is shown in Table.2. According to table.2, most of the RI sensors work in the visible and near-infrared bands, while the RI sensor we proposed works in the mid-infrared region, which is the vibration fingerprint band of molecules. For RI sensors based on metal materials such as gold and silver, the FoM is usually relatively low even less than 20 due to the existence of ohmic loss according to Ref. [25,26,34,44]. The FoM is improved in Ref. [24,28,35]-[38,45] but it is usually accompanied by a decrease in the sensitivity. It is maintained the high S and FoM value of the sensor in Ref. [39] but the resonance strongly depends on the incident angle, while the sensor we proposed is incident angle-independent. The FoM* of the Ref. [40] can be as high as 13,500

Table 2
RI sensors based on Fano resonance in the last five years. "–" means not mentioned. "*" means it is calculated in a different way.

Year [Ref.]	Materials	Unit structure	Peak Position (nm)	RI range (resolution)	S (nm/RIU)	FoM (RIU^{-1})	Q	Polariz-ation	Incident angle
2015 [24]	Au	Nano-mushroom	827	1.333–1.413	565	35	–	–	–
2015 [25]	Au	Split ring	820	1.0–1.4	325	10.8	–	–	dependent
2015 [26]	Au	U-type nanograter	1620	1.0–1.32 (0.02)	2040	12.5	–	Insensi-tive	–
2016 [40]	Ag	MIM waveguide	964	1.0–1.5	938	13500*	–	–	–
2017 [35]	Au	grating	699	1.333–1.350	470	31	–	–	–
2017 [41]	SOI	PCRR	1550	1.3315–1.3335	366	–	–	sensitive	–
2017 [42]	SOI	PC	1537	1.33 (1.3E-6)	264	–	10,000	–	–
2018 [39]	Au	2D hexagon	810	1.333–1.336	5833	730	–	–	dependent
2018 [36]	Si	nanobar pairs	1150	1.333–1.339	370	2846	Exceed 10E5	–	–
2018 [44]	Au	nanoholes	656	1–1.33	615	–	–	insenstive	–
2019 [37]	Si3N4, SiO2	Grating-waveguide	602.5	1.4–1.7	110	190	–	Insensi-tive	–
2019 [43]	Si, InAs	fiber	9000	1.0–1.7 (0.00012)	1695	–	–	–	
2019 [45]	Si	nanobars	855	–	263	–	144	–	–
2020 [35]	Si, glass	elliptical ring-disks	999	1.3–1.4	541	2353	4350	sensitive	dependent
2020 [25]	Si, SiO2	elliptical disk and ring	860	1.32–1.36	392	3001	7421	sensitive	–
2020 [31]	Ag	MIM waveguide	1651	1.4–1.5	1556	14.83	16.18	–	–
This paper	Si	lucky knot	7300	1.33–2.0 (0.001)	986	32.7	520	Insensi-tive	Indepen-dent

because of the different calculation methods. The FOM* is defined as $FOM^{*} = \frac{\Delta T}{(T\Delta n)}$ where T denotes the transmittance of the proposed structure [40]. In summary, the RI sensor based on "lucky knot" nanostructure of dielectric materials proposed in this paper can effectively improve the FoM (32.7 RIU^{-1}) and Q (520) value while maintaining relatively high sensitivity (986 nm/RIU) compared to the optical RI sensors based on metallic materials. At the same time, it is insensitive to polarization and incident angle of the light.

RI of glucose solution at different temperatures

Based on the above-mentioned RI sensing performance, we simulated the RI changes of a 20% glucose solution at different temperatures from 25 to 60 degrees as shown in Fig. 8. It can be seen from Fig. 8 that the RI sensor designed in this paper can easily detect the change in RI of the glucose solution as temperature rises. Since the mid-infrared band is molecular vibration band, the nanostructure designed in this paper may provide a further step in biosensors.

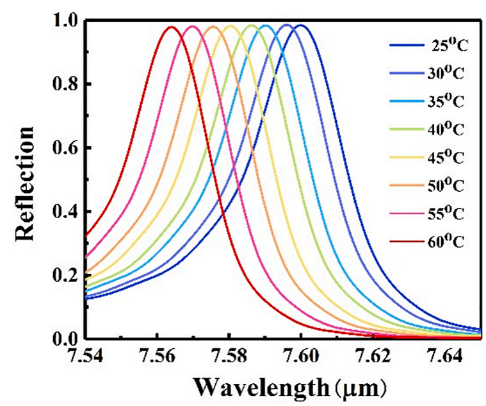

Fig. 8. The change of RI of glucose solution as temperature rises.

Conclusion

In this paper, we propose and discuss the resonance characteristics of the "lucky knot" shaped nanostructure based on all-dielectric materials using FDTD method. The interaction of the cross-rods structure and the ring structures in the "lucky knot" can achieve high-Q Fano resonance in the mid-infrared region. The dielectric nanostructure proposed in this paper is sensitive to changes in the RI of the environment. By analyzing the reflection spectra and near-field electromagnetic distribution, we find that the sensing sensitivity is as high as 986 nm/RIU, the maximum Q factor is as high as 520, the maximum FoM is 32.7 RIU^{-1} and the dephasing time is only 1.8 ps. In addition, it is insensitive to polarization and incident angle. When the polarization and the incident angle of the light is changed, the resonance is still there with a high reflectance and a narrow linewidth. Due to the use of dielectric materials, the FoM which is usually low when using metallic materials is improved, and it is compatible with the developed CMOS process, making it hopeful for large-scale integrated production. This research can be applied to other devices such as optical sensors, biological sensors and environmental monitors.

Funding

This work was supported by the grants from National Natural Science Foundation of China (Grant Numbers 61735018 and 61805242); Scientific and Technological Development Project of Jilin province (Grant Number 20190103014JH); Excellent Member of Youth Innovation Promotion Association CAS (Grant Numbers. Y201836, 2014193); Leading Talents and Team Project of Scientific and Technological Innovation for Young and Middle-aged Groups in Jilin Province (20190101012JH); Project of CIOMP-Duke Collaborative Research (201903002); Project of CIOMP-Fudan University Collaborative Research.

Declaration of Competing Interest

The authors declare that they have no known competing financial interests or personal relationships that could have appeared to influence the work reported in this paper.

References

[1] Xie Y, Liu X, Li F. Ultra-wideband enhancement on mid-infrared fingerprint sensing for 2D materials and analytes of monolayers by a metagrating. Nanophotonics 2020;20200180. https://doi.org/10.1515/nanoph-2020-0180.

[2] Yea Y, Xieb M, Ouyangb J, Tanga J. Tunable mid-infrared refractive index sensor with high angular sensitivity and ultra-high figure-of-merit based on Dirac semimetal. Results Phys 2020;17:103035. https://doi.org/10.1016/j.rinp.2020.103035.

[3] Tingting WU, Yu LUO, Lei WEI. Mid-infrared sensing of molecular vibrational modes with tunable graphene plasmons. Opt Lett 2017;42(11):2066. https://doi.org/10.1364/OL.42.002066.

[4] Yesilkoy F, Terborg RA, Pello J, Belushkin AA, Jahani Y, Pruneri V, et al. Phase-sensitive plasmonic biosensor using a portable and large field-of-view interferometric microarray imager. Light Sci Appl 2018;7(2):17152. https://doi.org/10.1038/lsa:2017.152.
[5] Kassa-Baghdouche L, Cassan E. Mid-infrared refractive index sensing using optimized slotted photonic crystal waveguides. Photonics Nanostruct Fundam Appl 2017. https://doi.org/10.1016/j.photonics.2017.11.001.
[6] Yuan-Fong Chou Chau. Mid-infrared sensing properties of a plasmonic metal-insulator-metal waveguide with a single stub including the defects. J Phys D: Appl Phys 2019. https://doi.org/10.1088/1361-6463/ab5ec3.
[7] Kassa-Baghdouche L. Optical properties of a point-defect nanocavity-based elliptical-hole photonic crystal for mid-infrared liquid sensing. Phys Scr 2020;95 (1):015502. https://doi.org/10.1088/1402-4896/ab474a.
[8] Bontempi N, Chong KE, Orton HW, Staude I, Choi D-Y, Alessandri I, et al. Highly sensitive biosensors based on all-dielectric nanoresonators. Nanoscale 2017;9(15): 4972–80. https://doi.org/10.1039/C6NR07904K.
[9] Yavas O, Svedendahl M, Dobosz P, Sanz V, Quidant R. On-a-chip biosensing based on all-dielectric nanoresonators. Nano Lett 2017;17(7):4421–6. https://doi.org/10.1021/acs.nanolett.7b0151810.1021/acs.nanolett.7b01518.s001.
[10] Yildirim DU, Ghobadi A, Soydan MC, Atesal O, Toprak A, Caliskan MD, et al. Disordered and densely packed ITO nanorods as an excellent lithography- free optical solar reflector metasurface. ACS Photon 2019;6(7):1812–22. https://doi.org/10.1021/acsphotonics.9b0063610.1021/acsphotonics.9b00636.s001.
[11] Soydan MC, Ghobadi A, Yildirim DU, Erturk VB, Ozbay E. All ceramic- based metal-free ultra-broadband perfect absorber. Plasmonics 2019;14(6):1801–15. https://doi.org/10.1007/s11468-019-00976-z.
[12] Mahmoudi M, Lohse SE, Murphy CJ, Fathizadeh A, Montazeri A, Suslick KS. Variation of protein corona composition of gold nanoparticles following plasmonic heating. Nano Lett 2014;14(1):6–12. https://doi.org/10.1021/nl403419e.
[13] Yildirim DU, Ghobadi A, Soydan MC, Gokbayrak M, Toprak A, Butun B, et al. Colorimetric and near-absolute polarization-insensitive refractive-index sensing in all-dielectric guided-mode resonance based metasurface. J Phys Chem C 2019;123 (31):19125–34. https://doi.org/10.1021/acs.jpcc.9b04748.
[14] Zhang J, MacDonald KF, Zheludev NI. Near-infrared trapped mode magnetic resonance in an all-dielectric metamaterial. Optics Express 2013;21(22):26721. https://doi.org/10.1364/OE.21.026721.
[15] Zhang J, Liu W, Zhu Z, Yuan X, Qin S. Strong field enhancement and light-matter interactions with all-dielectric metamaterials based on split bar resonators. Opt Express 2014;22(25):30889. https://doi.org/10.1364/OE.22.030889.
[16] Cao Z, Yao Baicheng. Biochemical sensing in graphene-enhanced microfiber resonators with individual molecule sensitivity and selectivity. Light Sci Appl 2019;8:107. https://doi.org/10.1038/s41377-019-0213-3.
[17] Mazdak T. Trends in graphene research. Mater Today 2009;12(10):34–7. https://doi.org/10.1016/S1369-7021(09)70274-3.
[18] Lin Li, Peng H, Liu Z. Synthesis challenges for graphene industry. Nat Mater 2019; 18(6):520–4. https://doi.org/10.1038/s41563-019-0341-4.
[19] Zhu Z, Bai B, You O, Li Q, Fan S. Fano resonance boosted cascaded optical field enhancement in a plasmonic nanoparticle-in-cavity nanoantenna array and its SERS application. Light-Sci Appl 2015;4(6):e296. https://doi.org/10.1038/lsa:2015.69.
[20] Zhang F, Huang X, Zhao Q. Fano resonance of an asymmetric dielectric wire pair. Appl Phys Lett 2014;105(172901). https://doi.org/10.1063/1.4900757.
[21] Shah YD, Grant J, Hao D, Kenney M, Pusino V, Cumming DRS. Ultra-narrow line width polarization-insensitive filter using a symmetry-breaking selective plasmonic metasurface. ACS Photon 2018;5(2):663–9. https://doi.org/10.1021/acsphotonics.7b01011.
[22] Cong S, Liu X, Jiang Y, Zhang W, Zhao Z. Surface enhanced raman scattering revealed by interfacial charge-transfer transitions. Innovation 2020;1(3):100051. https://doi.org/10.1016/j.xinn.2020.100051.
[23] Xuan Z, Li J, Liu Q, Yi F, Wang S, Lu W. Artificial structural colors and applications. Innovation 2021. https://doi.org/10.1016/j.xinn.2021.100081.
[24] Li W, Xue J, Jiang X, Zhou Z, Ren K, Zhou J. Low-cost replication of plasmonic gold nanomushroom arrays for transmission-mode and multichannel biosensing. RSC Adv 2015;5(75):61270–6. https://doi.org/10.1039/C5RA12487E.
[25] Bao Y, Hu Z, Li Z, Zhu X, Fang Z. Plasmonic Fano resonance at optical frequency. Small 2015;11(18):2177–81.
[26] Cui A, Liu Z, Li J, Shen TH, Xia X, Li Z, et al. Directly patterned substrate-free plasmonic "nanograter" structures with unusual Fano resonances. Light Sci Appl 2015;4(7):e308. https://doi.org/10.1038/lsa:2015.81.
[27] Popa BI, Cummer SA. Compact dielectric particles as a building block for low-loss magnetic metamaterials. Phys Rev Lett 2008;100:207401. https://doi.org/10.1103/PhysRevLett.100.207401.
[28] Wei Su, Chenb X, Gengb Z. Multiple Fano resonances in all-dielectric elliptical disk-ring metasurface for high-quality refractive index sensing. Results Phys 2020;18: 103340. https://doi.org/10.1016/j.rinp.2020.103340.
[29] Baranov DG, Zuev DA, Lepeshov SI, Kotov OV, Krasnok AE, Evlyukhin AB, et al. All-dielectric nanophotonics: the quest for better materials and fabrication techniques. Optica 2017;4(7):814. https://doi.org/10.1364/OPTICA.4.000814.
[30] Palik ED. Handbook of Optical Constants of Solids. Academic; 1997.
[31] Yang Y, Kravchenko II, Briggs DP, Valentine J. All-dielectric metasurface analogue of electromagnetically induced transparency. Nat Commun 2014;5(1). https://doi.org/10.1038/ncomms6753.
[32] Xu Yi, Bai P, Zhou X, Akimov Y, Png CE, Ang L-K, et al. Optical refractive index sensors with plasmonic and photonic structures: promising and inconvenient truth. Adv Optical Mater 2019;7(9):1801433. https://doi.org/10.1002/adom.v7.910.1002/adom.201801433.
[33] Zhang Y, Liang Z. A long wavelength infrared narrow-band reflection filter based on an asymmetric hexagonal structure. Optics Commun 2020;475. https://doi.org/10.1016/j.optcom.2020.126264.
[34] Sagor Rakibul Hasan, Farhad Hassan Md. Numerical investigation of an optimized plasmonic on-chip refractive index sensor for temperature and blood group detection. Results Phys 2020;19:103611. https://doi.org/10.1016/j.rinp.2020.103611.
[35] Wang Y, Sun C, Li H, Gong Q, Chen J. Self-reference plasmonic sensors based on double Fano resonances. Nanoscale 2017;9(31):11085–92. https://doi.org/10.1039/C7NR04259K.
[36] Zhang Yuebian, Liu Wenwei. High-quality-factor multiple Fano resonances for refractive index sensing. Opt Lett 2018;43(8):1842. https://doi.org/10.1364/OL.43.001842.
[37] Yildirim DU, Ghobadi A, Soydan MC, Gokbayrak M, Toprak A, Butun B, et al. Colorimetric and near-absolute polarization-insensitive refractive-index sensing in all-dielectric guided-mode resonance based metasurface. J Phys Chem C 2019;123 (31):19125–34. https://doi.org/10.1021/acs.jpcc.9b04748.
[38] Wei S, Ding Y. A high figure of merit refractive index sensor based on Fano resonance in alldielectric metasurface. Results Phys 2020;16:102833. https://doi.org/10.1016/j.rinp.2019.102833.
[39] Liu B, Chen S, Zhang J, Yao X, Zhong J, Lin H, et al. A plasmonic sensor array with ultrahigh figures of merit and resonance linewidths down to 3 nm. Adv Mater 2018;30(12):1706031. https://doi.org/10.1002/adma.v30.1210.1002/adma.201706031.
[40] Binfeng Y, Hu G, Zhang R, Yiping C. Fano resonances in a plasmonic waveguide system composed of stub coupled with a square cavity resonator. J Opt 2016;18(5): 055002. https://doi.org/10.1088/2040-8978/18/5/055002.
[41] Zhengrui TU, Dingshan GAO, Zhang Meiling. High-sensitivity complex refractive index sensing based on Fano resonance in the subwavelength grating waveguide micro-ring resonator. Opt Express 2017;25(17):20911. https://doi.org/10.1364/OE.25.020911.
[42] Wang S, Liu Y, Zhao D. Optofluidic Fano resonance photonic crystal refractometric sensors. Appl Phys Lett 2017;110:091105. https://doi.org/10.1063/1.4977563.
[43] Zhoua X, Yua Q, Peng W. Mid-infrared surface plasmon resonance sensor based on silicon-doped InAs film and chalcogenide glass fiber. Opt Laser Technol 2019;120: 105686. https://doi.org/10.1016/j.optlastec.2019.105686.
[44] Yesilkoy F, Arvelo ER, Jahani Y, Liu M, Tittl A, Cevher V, et al. Ultrasensitive hyperspectral imaging and biodetection enabled by dielectric metasurfaces. Nat Photon 2019;13(6):390–6.
[45] Yesilkoy F, Terborg RA, Pello J, Belushkin AA, Jahani Y, Pruneri V, et al. Phase-sensitive plasmonic biosensor using a portable and large field-of-view interferometric microarray imager. Light Sci Appl 2018;7(2):17152. https://doi.org/10.1038/lsa:2017.152.